S-matrix poles near the ΛN and ΣN Thresholds in the Coupled $\Lambda N - \Sigma N$ System

K. Miyagawa and H. Yamamura
Department of Applied Physics, Okayama University of Science
1-1 Ridai-cho, Okayama 700, Japan
(February 9, 2008)

Abstract

We search t-matrix poles for $\Lambda N - \Sigma N$ coupling interactions using two soft core models of the Nijmegen group which bind the hypertriton at the correct binding energy, and hard core models which are still influential in hypernuclear physics. To treat the hard core potentials, a useful method for calculating the off-shell t-matrix is proposed. We find poles close to the ΣN threshold in the second or third quadrant of the complex plane of the ΣN relative momentum. The relation between the poles and the shape of the ΛN elastic total cross section is discussed based on a so-called uniformization by which two-channel t-matrices become single-valued on a complex valuable. We also find poles near the ΛN threshold. These are correlated to the S-wave ΛN scattering lengths, the values of which have yet to be determined.

13.75.Ev, 21.45.+v, 21.30.-x, 21.80+a

I. INTRODUCTION

Most of our knowledge of the YN interaction has been obtained from heavy hypernuclei and it remains rather qualitative. In contrast, recent theoretical analyses of few-baryon systems with strangeness such as the three-body calculations of ${}^{3}_{\Lambda}H$ [1–3] and the four-body study of ${}^{4}_{\Lambda}H$ [4] yield more qualitative results, being based on modern baryon-baryon forces and on rigorous solutions of the few-body Schrödinger equations. Thus, they offer a great advantage to scrutinize YN interaction models. As an example, Refs. [1–3] demonstrated that the Nijmegen soft core YN interaction NSC89 [5] binds the hypertriton, but the Jülich $\tilde{A}$ potential [6] does not. This is possibly caused by the sizable difference between the ${}^1S_0$ force components in the low-energy region [2]. This shows that even basic quantities such as scattering lengths are still undetermined.

The few-body analysis of ${}^{3}_{\Lambda}H$ [1–3] has also clarified the effect of the $\Lambda - \Sigma$ conversion which was exactly included in the coupled channel formalism [1]. Although in the case of the hypertriton the admixture of ΣNN states is only 0.5%, the expectation values of the sum of the transition potentials $V_{\Lambda N,\Sigma N}$ and $V_{\Sigma N,\Lambda N}$ are approximately 8% of the total potential energy, which is crucial for the binding of the hypertriton [2,3].

This knowledge about the Σ states coupling, however, has been obtained from the bound state lying below the ΛNN threshold. This should be extended to analyses close to the Σ threshold, where $\Lambda - \Sigma$ conversion effects will emerge sharply. In this region, so-called unstable bound states [7] have received attention and have been searched for experimentally. Only one state in the $\Sigma(\Lambda)NNN$ system is confirmed in the reaction ${}^4He(K^-,\pi^-)$ [8]. The existence of such an unstable bound state in the A=4 system was predicted by Harada *et al.* where the coupling to continuum ΛNNN states was approximated by a ΣN optical potential [9]. However, for understanding the actual features of $\Lambda-\Sigma$ conversion, it is highly desirable to treat it directly using a realistic $\Lambda N - \Sigma N$ coupling interaction.

At present, it is technically possible to incorporate precisely the coupling to Λ continuum states for only the ΣN and ΣNN systems. Afnan and Gibson [10] calculated the Λd elastic scattering fully incorporating this coupling but using simple phenomenological YN interactions. They then found and analyzed enhancements just below the ΣNN threshold. To examine more closely the $\Lambda N - \Sigma N$ coupling interaction, a similar study applying more sophisticated meson-theoretical interactions is necessary. It is also important to analyze electromagnetic hyperon-production processes [11], which are experimentally accessible.

For the YN interaction, there exists a variety of strengths for the $\Lambda N - \Sigma N$ coupling among extensively used meson-theoretical potentials. The soft core model [5] and the hard core model D [12] of the Nijmegen group show cusps in the ΛN elastic total cross section just at the ΣN threshold with different magnitudes, while the Nijmegen hard core model F [13] and the Jülich models [6] show round resonance peaks below the threshold. We stress here that these prominent cusps do not mean simple threshold effects, but suggest the existence of t-matrix poles in unphysical Riemann sheets. This is important because the poles might move and become unstable bound state poles if the coupling strengths varied. Some examples for separable potentials are given in Ref. [14]. In this paper, we shall locate these poles and follow their trajectories for the Nijmegen potentials.

Knowledge of YN t-matrix around the ΣN threshold is crucial for the analysis of $\Lambda NN-\Sigma NN$ continuum states using meson-theoretical interactions. This paper accordingly

investigates poles of the t-matrices for the Nijmegen F, D and the two soft core interactions [5,15]. This is achieved in momentum space and hence the results are directly applicable to the three-body calculation. The behavior of t-matrices around an inelastic threshold in coupled channel problems and the effects of nearby poles have often been studied [7,14]. In such analyses it is important to understand the connection between various Riemann energy sheets and how far from the physical region the poles are located. In this analysis we adopt a so-called uniformization given by Newton [16], by which the t-matrix for two-channel problems becomes single-valued after a suitable variable is introduced in place of energy. We thereby clearly describe the positions and the trajectories of the t-matrix poles in the Riemann sheets.

Section II gives the expression for $\Lambda N - \Sigma N$ t-matrix which is analytically continued to the complex energy plane. Section III describes a method to treat a hard core potential in momentum space. This is for the purpose of treating the Nijmegen hard core potentials which are influential in hypernuclear physics. In Sec. IV, the uniformization mentioned above is introduced, thereby we discuss how the shape of the ΛN elastic total cross section around the ΣN threshold is related to the positions of nearby poles. In Sec. V, the positions of the t-matrix poles for the Nijmegen soft and hard core models are described. We also show the trajectories of the poles when the strengths of the potentials are increased.

II. ANALYTIC CONTINUATION OF THE T-MATRIX

In this section, we give the expression of the off-shell t-matrix for the $\Lambda N - \Sigma N$ system and continue it analytically into the complex energy plane.

The coupled t-matrices for the $\Lambda N - \Sigma N$ system are defined by the integral equations

$$T_{ij}(z) = V_{ij} + \sum_k V_{ik}\, G_0^{(k)}(z)\, T_{kj}(z), \qquad i,j,k = 1,2 \tag{2.1}$$

with

$$G_0^{(k)}(z) = \left(z - H_0^{(k)}\right)^{-1}, \qquad z = E + i\varepsilon \tag{2.2}$$

where i, j, k have integer values of 1 and 2 for the ΛN and ΣN channels, respectively. The free Hamiltonian $H_0^{(k)}$ for channel k is defined as

$$H_0^{(k)} = \frac{p_k^2}{2\mu_k} + m_N + m_Y^{(k)}\,. \tag{2.3}$$

This refers to the total momentum zero frame and we denote the relative momentum between the nucleon and the hyperon by $\mathbf{p_k}$ and the reduced mass of channel k by μ_k. The masses $m_Y^{(k)}(k = 1, 2)$ indicate m_Λ and m_Σ respectively. After performing the partial-wave decomposition in momentum space, we express the projected t-matrix elements for a given total angular momentum and parity again by T. Then Eq. (2.1) reads

$$< p \,|\, T_{ij}(z) \,|\, p' > \; = < p \,|\, V_{ij} \,|\, p' >$$

$$+ \sum_k \int_0^\infty dp'' p''^2 < p \,|\, V_{ik} \,|\, p'' > \frac{1}{e_k - \frac{p''^2}{2\mu_k} + i\varepsilon} < p'' |\, T_{kj}(z) |\, p' > \qquad (2.4)$$

with

$$e_k \equiv \frac{q_k^2}{2\mu_k} = E - m_N - m_Y^{(k)} \ . \qquad (2.5)$$

To simplify the notation, the p indices have been omitted, and the partial-wave elements are assumed to have no coupling between different orbital angular momenta or channel-spin states. The extension to the case with couplings is straightforward.

Now consider the energy E to be a complex number. Hence e_k and

$$q_k = \sqrt{2\mu_k e_k} \qquad (2.6)$$

are complex numbers. We introduce the function

$$h_k(p'') \equiv < p \,|\, V_{ik} \,|\, p'' >< p'' \,|\, T_{kj}(z) \,|\, p' > \qquad (2.7)$$

and define each term in the $k-$summation of the right-hand side of Eq. (2.4) by $I_k(e_k)$ as

$$I_k(e_k) = \int_0^\infty dp'' \ \frac{p''^2 h_k(p'')}{e_k - \frac{p''^2}{2\mu_k}} \ . \qquad (2.8)$$

This function has a cut for $e_k \geq 0$, in other words, a cut along $m_N + m_Y^{(k)} \leq E < \infty$. Thus, there are two cuts in the E plane starting at the $N + \Lambda$ and $N + \Sigma$ thresholds, respectively. The function values beyond the cuts are defined by analytic continuation. This is achieved by modifying Eq. (2.8) as

$$I_k(e_k) = \int_0^\infty dp'' \ \frac{p''^2 h_k(p'') - 2\mu_k e_k h_k(q_k)}{e_k - \frac{p''^2}{2\mu_k}} + h_k(q_k) \int_0^\infty dp'' \frac{2\mu_k e_k}{e_k - \frac{p''^2}{2\mu_k}} \qquad (2.9)$$

where we assume that $h_k(p)$ can be continued analytically and has no singularity in the trajectory from real p to the complex value q_k given in Eq. (2.6). This is true for the case here. The cut now appears explicitly in the second term of Eq. (2.9). It is then easy to show

$$\int_0^\infty dp'' \frac{2\mu_k e_k}{e_k - \frac{p''^2}{2\mu_k}} \ = -i\pi\mu_k \sqrt{2\mu_k e_k} = -i\pi\mu_k q_k \qquad (2.10)$$

which defines the integral in both sheets of the Riemann e_k surface, corresponding to positive and negative imaginary parts of q_k. From Eqs. (2.9) and (2.10), we can rewrite Eq. (2.4) as

$$
\begin{aligned}
&< p \,|\, T_{ij}(z) \,|\, p' >=< p \,|\, V_{ij} \,|\, p' > \\
&+ \sum_k \left[\int_0^\infty dp'' \left(\frac{p''^2 < p \,|\, V_{ik} \,|\, p'' >< p'' \,|\, T_{kj}(z) \,|\, p' >}{e_k - \frac{p''^2}{2\mu_k}} \right.\right. \\
&\left.\left. - \frac{2\mu_k e_k < p \,|\, V_{ik} \,|\, q_k >< q_k \,|\, T_{kj}(z) \,|\, p' >}{e_k - \frac{p''^2}{2\mu_k}} \right) - i\pi\, \mu_k q_k < p \,|\, V_{ik} \,|\, q_k >< q_k \,|\, T_{kj}(z) \,|\, p' > \right].
\end{aligned}
\tag{2.11}
$$

This equation contains a new t-matrix element $< q_k \mid T_{kj} \mid p' >$ which requires the additional equation

$$
\begin{aligned}
&< q_k \,|\, T_{ij}(z) \,|\, p' >=< q_k \,|\, V_{ij} \,|\, p' > \\
&+ \sum_k \left[\int_0^\infty dp'' \left(\frac{p''^2 < q_k \,|\, V_{ik} \,|\, p'' >< p'' \,|\, T_{kj}(z) \,|\, p' >}{e_k - \frac{p''^2}{2\mu_k}} \right.\right. \\
&\left.\left. - \frac{2\mu_k e_k < q_k \,|\, V_{ik} \,|\, q_k >< q_k \,|\, T_{kj}(z) \,|\, p' >}{e_k - \frac{p''^2}{2\mu_k}} \right) - i\pi\, \mu_k q_k < q_k \,|\, V_{ik} \,|\, q_k >< q_k \,|\, T_{kj}(z) \,|\, p' > \right].
\end{aligned}
\tag{2.12}
$$

The Eqs. (2.11) and (2.12) form a closed set of integral equations [17] and define the t-matrix elements on the entire q_k planes or the Riemann surface of the complex energy E. This set is solved in the following sections.

III. T-MATRIX FOR A HARD CORE POTENTIAL

Although it is now rare to represent the short-range repulsion of the NN interaction by a hard core, the Nijmegen D and F models of the YN interaction with hard cores are still used frequently in hypernuclear physics. Therefore, in this section we explore a method to obtain the off-shell t-matrix for a hard core potential in momentum space.

The off-shell t-matrix can be expressed as

$$
< \vec{p} \,|\, T(z) \,|\, \vec{k} >=< \vec{p} \,|\, V \,|\, \Psi^{(+)}_{q,\vec{k}} > \tag{3.1}
$$

where $\Psi^{(+)}_{q,\vec{k}}$ is defined by

$$| \Psi^{(+)}_{q,\vec{k}} >= | \vec{k} > + G_0(z)\, V \,| \Psi^{(+)}_{q,\vec{k}} > \tag{3.2}$$

with

$$z = \frac{q^2}{2\mu} + i\varepsilon \ . \tag{3.3}$$

To simplify the notation, the $\Lambda N - \Sigma N$ coupling has been omitted. First, we divide the interaction V into the pure hard core part U and the remainder $\hat{V}$ as

$$V = U + \hat{V} \tag{3.4}$$

and use the two-potential formula [18] to obtain

$$< \vec{p}\,| \, T(z) \, | \, \vec{k} >=< \vec{p}\,| \, U \, | \, \Phi^{(+)}_{q,\vec{k}} > + < \Phi^{(-)}_{q,\vec{p}} \, | \, \hat{V} \, | \, \Psi^{(+)}_{q,\vec{k}} > \tag{3.5}$$

with

$$| \Phi^{(+)}_{q,\vec{k}} >= | \vec{k} > + G_0(z)\, U \,| \Phi^{(+)}_{q,\vec{k}} > \ , \tag{3.6}$$

$$| \Phi^{(-)}_{q,\vec{p}} >= | \vec{p} > + G_0(z^*)\, U \,| \Phi^{(-)}_{q,\vec{p}} > \ . \tag{3.7}$$

As we shall show later, the first term of the right-hand side of Eq. (3.5) is expressed analytically, and the second term satisfies an integral equation similar to the Lippmann-Schwinger equation which can be solved using a standard method. Our method is thus a natural extension of a standard treatment without a hard core, and is therefore useful not only for the present purpose, but also for other few-body calculations in momentum space.

The analytic expression of the first term in Eq. (3.5) has already been given by Takemiya [19], who proposed a method to evaluate the off-shell t-matrix for a hard-core potential in coordinate space. Here, we use this method only in the treatment of the pure hard-core part of the formula.

$\Phi^{(+)}_{q,\vec{k}}$ and $\Phi^{(-)}_{q,\vec{p}}$ in Eqs. (3.6) and (3.7) can be expanded into partial waves

$$\Phi^{(\pm)}_{q,\vec{k}}(\vec{r}) = \sum_{\substack{l's' \\ ls \\ JM}} \mathcal{Y}^{JM}_{l's'}(\hat{r})\, \Phi^{J(\pm)}_{l's'ls}(q,k,r)\, \mathcal{Y}^{JM\dagger}_{ls}(\hat{k}) \tag{3.8}$$

and similarly $\Psi^{(+)}_{q,\vec{k}}$. Here, y^{JM}_{LS} is the simultaneous eigenfunction of L^2, S^2, J^2 and J_z. We denote the pure-hard core part of Eq. (3.5) as

$$< \vec{p} \,|\, \tilde{t}(z) \,|\, \vec{k} > \equiv < \vec{p} \,|\, U \,|\, \Phi^{(+)}_{q,\vec{k}} > \tag{3.9}$$

and decompose it into partial waves

$$< \vec{p} \,|\, \tilde{t}(z) \,|\, \vec{k} > = \sum_{\substack{l's' \\ ls \\ JM}} y^{JM}_{l's'}(\hat{r})\, \tilde{t}^{J}_{l's'ls}(p,k;z)\, y^{JM\,\dagger}_{ls}(\hat{k}) \ . \tag{3.10}$$

Reference [19] proves that if we introduce a function χ defined by

$$\frac{\chi^{J(\pm)}_{l's'ls}(q,k,r)}{r}\sqrt{\frac{2}{\pi}}\, i^l \equiv \Phi^{J(\pm)}_{l's'ls}(q,k,r) - \sqrt{\frac{2}{\pi}}\, i^l j_l(kr) \tag{3.11}$$

it satisfies the equation

$$\left(q^2 + \frac{d^2}{dr^2} - \frac{l'(l'+1)}{r^2}\right) \chi^{J(\pm)}_{l's'ls}(q,k,r) - \sum_{l''s''} 2\mu\, U^{J}_{l's'l''s''}(r)\, \chi^{J(\pm)}_{l''s''ls}(q,k,r) = r 2\mu\, U^{J}_{l's'ls}(r)\, j_l(kr) \tag{3.12}$$

and the off-shell element of $\tilde{t}$ is given by χ as

$$\tilde{t}^{J}_{l's'ls}(p,k;z) = \frac{1}{2\mu}\,\frac{2}{\pi}\, i^{-l'+l} \int_0^\infty dr\, r\, j_{l'}(pr) \left(q^2 + \frac{d^2}{dr^2} - \frac{l'(l'+1)}{r^2}\right) \chi^{J(+)}_{l's'ls}(q,k,r) \ . \tag{3.13}$$

Following the method described in Ref. [19] one arrives at the analytic expression of the $\tilde{t}$ element in Eq. (3.13). For a pure hard core potential with radius c, Eq. (3.12) has the solution

$$\chi^{J(\pm)}_{l's'ls}(q,k,r) = \delta_{l'l}\delta_{s's} \times \begin{cases} -r\, j_l(kr) & (r \le c) \\ -\dfrac{j_l(kc)}{h^{(\pm)}_l(qc)}\, r\, h^{(\pm)}_l(qr) & (r \ge c) \end{cases} \tag{3.14}$$

Note, there is no coupling in ℓ and s, a result which can be found by generating the hard-core potential matrix U as limits of square well potentials (see Ref. [19]). Further, from Eq. (3.14) the integration in Eq. (3.13) is limited to $r \leq c$ and performing the integration we obtain the final expression for $\tilde{t}$

$$\begin{aligned}\tilde{t}^J_{l's'ls}(p,k;z) = \delta_{l'l}\delta_{s's}\,\frac{1}{2\mu}\,\frac{2}{\pi}\,i^{-l'+l} \\ \times\left[-\,c\,j_l(pc)\frac{d}{dr}\,r\,h_l^{(+)}(qr)\Big|_{r=c}\,\frac{j_l(kc)}{h_l^{(+)}(qc)} + \frac{d}{dr}\,r\,j_l(pr)\Big|_{r=c}\,c\,j_l(kc)\right. \\ \left. -\,\left(q^2-p^2\right)\int_0^c dr\,r^2\,j_l(pr)\,j_l(kr)\right]. \qquad (3.15)\end{aligned}$$

The last term on the right-hand side of this equation is shown in Ref. [19] to be

$$\int_0^c dr\,r^2\,j_l(pr)\,j_l(kr) = \begin{cases} \dfrac{c^2}{k^2-p^2}\left(\,k\,j_l(pc)\,j_{l+1}(kc) - p\,j_l(kc)\,j_{l+1}(pc)\right) & (p\neq k) \\ \dfrac{c^2}{2k}\left(\,k\,c\left(\,j_l^2(kc)+j_{l+1}^2(kc)\,\right) - (2l+1)\,j_l(kc)\,j_{l+1}(kc)\right) & (p=k) \end{cases} \qquad (3.16)$$

Next, let us consider the second part of the two-potential formula (3.5). The state $\Psi^{(+)}_{q,\vec{k}}$ given in Eq. (3.2) satisfies another equation [18]

$$|\,\Psi^{(+)}_{q,\vec{k}}> = |\,\Phi^{(+)}_{q,\vec{k}}> + G_U(z)\,\hat{V}\,|\,\Psi^{(+)}_{q,\vec{k}}> \qquad (3.17)$$

with

$$G_U(z) = G_0(z) + G_0(z)\,U\,G_U(z)\ . \qquad (3.18)$$

Hence, if we define $\hat{t}$ by

$$<\vec{p}\,|\,\hat{t}(z)\,|\,\vec{k}> \equiv <\Phi^{(-)}_{q,\vec{p}}\,|\,\hat{V}\,|\,\Psi^{(+)}_{q,\vec{k}}> \qquad (3.19)$$

then the second part of the two-potential formula becomes

$$< \vec{p} \,|\, \hat{t}(z) \,|\, \vec{k} > = < \Phi^{(-)}_{q,\vec{p}} \,|\, \hat{V} \,|\, \Phi^{(+)}_{q,\vec{k}} > + < \Phi^{(-)}_{q,\vec{p}} \,|\, \hat{V}\, G_U(z)\, \hat{V} \,|\, \Psi^{(+)}_{q,\vec{k}} > \ . \tag{3.20}$$

Observing that

$$\begin{aligned} < \vec{p}\,' \,|\, G_U &= < \vec{p}\,' \,|\, G_0 \,(\, 1 + U G_U \,) \\ &= \frac{1}{z - \frac{p'^2}{2\mu}} < \Phi^{(-)}_{q,\vec{p}\,'}| \end{aligned} \tag{3.21}$$

and applying it to the second term of the right-hand side of Eq. (3.20), we arrive at the integral equation for $\hat{t}$

$$< \vec{p} \,|\, \hat{t}(z) \,|\, \vec{k} > = < \Phi^{(-)}_{q,\vec{p}} \,|\, \hat{V} \,|\, \Phi^{(+)}_{q,\vec{k}} > + \int d\vec{p}\,' < \Phi^{(-)}_{q,\vec{p}} \,|\, \hat{V} \,|\, \vec{p}\,' > \frac{1}{z - \frac{p'^2}{2\mu}} < \vec{p}\,' \,|\, \hat{t}(z) \,|\, \vec{k} > \ . \tag{3.22}$$

The inputs to this integral equation, $< \Phi^{(-)}_{q,\vec{p}} \mid \hat{V} \mid \Phi^{(+)}_{q,\vec{k}} >$ and $< \Phi^{(-)}_{q,\vec{p}} \mid \hat{V} \mid \vec{p}\,' >$, are expressed by the scattering states from the pure hard-core part, $\Phi^{(\pm)}$, and the remainder of the potential, $\hat{V}$. From Eqs. (3.11) and (3.14), the scattering states $\Phi^{(\pm)}$ can be expressed simply by spherical Bessel and Hankel functions as

$$\Phi^{J(\pm)}_{l's'ls}(q,k,r) = \begin{cases} 0 & (r < c) \\ \delta_{l'l}\delta_{s's} \sqrt{\dfrac{2}{\pi}}\, i^l \left(j_l(kr) - \dfrac{j_l(kc)}{h^{(\pm)}_l(qc)}\, h^{(\pm)}_l(qr) \right) & (r > c) \end{cases} \tag{3.23}$$

allowing the inputs to be easily calculated. Thus, the integral equation (3.23) can be solved in a similar manner as described in Sec. II.

Consequently, combining the analytic expression given in Eqs. (3.15) and (3.16) with the solution of this integral equation, we easily obtain the off-shell t-matrix for a hard-core potential.

IV. CUSPS AND ROUND PEAKS CAUSED BY NEARBY POLES

As described in Sec. I, the main aim of this paper is to search t-matrix poles for various YN interactions around the ΣN threshold. In Eq. (2.4), the t-matrix elements are defined by the relative momenta between the hyperons and the nucleon, q_1 in the case of Λ-N and q_2 in the case of Σ-N. However, these momenta are not independent and are related to the energy E through Eq. (2.5). This can be rewritten as

$$\frac{q_1^2}{2\mu_1} + m_N + m_\Lambda = \frac{q_2^2}{2\mu_2} + m_N + m_\Sigma = E \ . \tag{4.1}$$

Thus, each t-matrix element is a function of the energy E, and has branch points at the two thresholds $E = m_N + m_\Lambda$ and $E = m_N + m_\Sigma$. We therefore encounter a somewhat complicated Riemann energy surface with four sheets, and must specify how they are related to the upper and lower halves of the q_1 and q_2 planes [7,14]. In two-channel problems, a procedure called uniformization [16] is very convenient to map the 4 Riemann sheets into one plane. This is used in the present analysis. The uniformization procedure introduces a new variable in place of the energy, in terms of which the t-matrix becomes single-valued. Following Ref. [16], we introduce such a variable ω which satisfies

$$\frac{q_1}{\sqrt{2\mu_1}} + \frac{q_2}{\sqrt{2\mu_2}} = \Delta \ \omega \tag{4.2}$$

and

$$\frac{q_1}{\sqrt{2\mu_1}} - \frac{q_2}{\sqrt{2\mu_2}} = \Delta \ \omega^{-1} \tag{4.3}$$

with

$$\Delta^2 \equiv m_\Sigma - m_\Lambda \ . \tag{4.4}$$

By these relations (4.3) and (4.2) it is easy to realize Eq. (4.1). These equations constitute a mapping of the Riemann energy surface to the complex ω plane which is shown in Fig. 1. Of course, there are 4 possible quadrants where q_1 can be located, and for each q_1 two different values of q_2 are allowed by Eq. (4.1). Hence, there are 8 possible cases in specifying to which quadrants both q_1 and q_2 belong on their own complex planes. The complex ω plane in Fig. 1 is divided accordingly into 8 parts, each of which contains two numbers inside square brackets indicating the quadrants to which q_1 and q_2 belong. The bold line expresses the region where bound or scattering states exist if present. The ΛN threshold is located at $\omega = i$, and the ΣN threshold resides at $\omega = 1$. If moving counter-clockwise around $\omega = i$, the quadrant to which q_1 belongs changes as $1 \to 2 \to 3 \to 4$, and at the same time the quadrant of q_2 changes as $1 \to 2 \to 1 \to 2$. On the other hand, if one moves around $\omega = 1$ which corresponds to the ΣN threshold, the quadrant to which q_2 belongs varies as $1 \to 2 \to 3 \to 4$ and the quadrants of q_1 as $1 \to 4 \to 1 \to 4$.

Let us now consider the relation between the shapes of the ΛN elastic total cross section and the positions of a pole near the ΣN threshold. One important difference to single channel problems is that there exists the region [1,3] touching the ΣN threshold. Suppose a pole exists in this region close to the threshold, then the ΛN elastic total cross section takes the shape of a cusp just at the threshold. On the other hand, if a pole resides in the region [4,2] or [4,4] close to the bold line mentioned above, the cross section shows a round peak of the Breit-Wigner form. A pole lying in the region [4,2] is often called an unstable bound state (UBS) pole [7].

We shall now discuss the above mentioned behavior of the cross sections. Assuming that the t-matrix has a pole at the position $(q_1, q_2) = (\alpha_1, \alpha_2)$ and the corresponding energy is E_0, it follows that

$$E_0 = \frac{\alpha_1^2}{2\mu_1} + m_N + m_\Lambda = \frac{\alpha_2^2}{2\mu_2} + m_N + m_\Sigma \ . \tag{4.5}$$

Then, the t-matrix elements around the pole can be approximated as

$$< p \,|\, T_{ij}(E) \,|\, p' > \simeq \frac{R_{ij}(p,p')}{E - E_0} \, . \tag{4.6}$$

The approximation (4.6) of a first-order pole holds even in the case when the pole resides in Riemann sheets other than the first, which is proved for example in Ref. [20] for a single channel case. The extension to the coupled $\Lambda N - \Sigma N$ system is straightforward. Notice, however, for all pairs of $(q_1, q_2) = (\pm\alpha_1, \pm\alpha_2)$ the energies defined by Eq. (4.1) take the same value E_0 but reside in different places on the Riemann energy surface. The approximation (4.6) is therefore valid only around $(q_1, q_2) = (\alpha_1, \alpha_2)$.

From Eqs. (4.1) and (4.5), we can rewrite Eq. (4.6) as

$$< p \,|\, T_{ij}(E) \,|\, p' > \simeq \frac{\tilde{R}_{ij}(p,p')}{q_1 - \alpha_1} \tag{4.7}$$

or

$$< p \,|\, T_{ij}(E) \,|\, p' > \simeq \frac{\bar{R}_{ij}(p,p')}{q_2 - \alpha_2} \ . \tag{4.8}$$

However, the expression (4.7) is not appropriate around the ΣN threshold. As already mentioned, this is because if the pole moves around the ΣN threshold, the quadrant to which α_1 belongs changes as $1 \to 4 \to 1 \to 4$, while the quadrant in which α_2 is located changes as $1 \to 2 \to 3 \to 4$. Therefore, the expression (4.7) can not distinguish whether the pole is situated in the regions [4,2] or [4,4], or in the regions [1,1] or [1,3]. On the other hand, the expression (4.8) can distinguish between the regions and so will be used here.

Let us now infer from Eq. (4.8) the shapes of the ΛN elastic total cross section σ around the ΣN threshold. Since

$$\sigma \propto | < q_1 \,|\, T_{11}(E) \,|\, q_1 > |^2 \tag{4.9}$$

the q_2 dependence of the cross section becomes roughly

$$\sigma \propto \left| \frac{1}{q_2 - \alpha_2} \right|^2 . \tag{4.10}$$

Writing $\alpha_2 = a + ib$, we have

$$\sigma \propto \begin{cases} \dfrac{1}{(|q_2| - b)^2 + a^2} & (\ q_2 = i|q_2| : \ \text{below the } \Sigma\text{N threshold }) \\ \\ \dfrac{1}{(q_2 - a)^2 + b^2} & (\ q_2 > 0 : \ \text{above the } \Sigma\text{N threshold}) \end{cases} \tag{4.11}$$

For the three cases, when the pole is located in the regions [4,2], [1,3] and [4,4], we plot the cross sections σ expressed by Eq. (4.11) in Figs. 2, 3 and 4, respectively. Notice that Figs. 2(c), 3(c) and 4(c) show the cross section as a function of the energy E, hence its derivative at the threshold energy is infinite according to the relation (4.1). If the pole is located in the regions [4,2] or [4,4], the cross sections show round peaks of the Breit-Wigner form (Figs. 2(c) or 4(c)), and are quite similar to the resonances in single channel problems. In contrast, if the pole sits in the region [1,3], the cross section forms a large cusp just at the threshold (Fig. 3(c)). In Ref. [7], these types of poles are named inelastic virtual state poles. We should recognize that such a large cusp is caused by the pole, and is not a simple threshold effect. Some such poles, as we shall show in the next section, can actually move into the region [4,2] and convert to unstable bound state poles when the potential strength is slightly increased.

V. RESULTS AND DISCUSSIONS

We searched t-matrix poles for various meson theoretical YN interactions in the manner described in Secs. II and III. We used two soft core models of the Nijmegen group, NSC89 [5] and the recently proposed new soft core model NSC97 [15], which includes six different versions named a, b, c, d, e and f. In this study we analyzed NSC97f. Both soft core models NSC89 and NSC97f reproduce the correct binding energy of the hypertriton [2,3,21]. We also chose hard core models D [12] and F [13] of the Nijmegen group (abbreviated as ND and NF respectively) which are still used in hypernuclear physics studies.

Fig. 5 shows the ΛN elastic total cross sections around the ΣN threshold for the force models above. The model NF yields a round peak, while ND and NSC89 form cusps just at the threshold. For NSC97f, the shape is unclear. All the enhancements are found to be caused by the ${}^3S_1 - {}^3D_1$ force component. Unfortunately, there exist only sparse experimental data of the ΛN cross sections, and so we can not determine its actual shape. However, a prominent peak around the ΣN threshold has been observed in the $K^- + d \to p + \Lambda + \pi^-$ reaction [22].

For every potential used, we found a pole near the ΣN threshold in the ${}^3S_1 - {}^3D_1$ wave. These are shown in Table I. In Fig. 6, the poles are also displayed in the complex q_2 ($\Sigma - N$ relative momentum) plane. For NSC97f and NF, the poles are located in the [4,2] region of the ω plane, and for NSC89 and ND, they lie in the region [1,3]. The relation between the position of the pole and the shape of the $\Lambda - N$ cross section described in Sec. IV holds for all potentials except NSC97f. The pole for NSC97f is close to the boundary between the regions [4,2] and [1,3], and it is farther from the imaginary axis of the q_2 plane than for NF. This explains why the shape of the ΛN cross sections for this potential is not a definite example of a cusp or a round peak type.

For all the interaction models, the poles are close to the ΣN threshold and cause some enhancements. For NSC97f, the unstable bound state exists in the two-body YN system, and very likely in the YNN system. We should emphasize that the poles in the region [1,3] which produce the cusps are as equally important as those in the region [4,2]. To demonstrate this, we calculated the trajectory of the pole for the potential ND, multiplying it by an overall strength parameter λ. The trajectory is shown in Fig 7. The pole moves from the region [1,3] into [4,2] as the potential strength increases, and becomes an unstable bound state pole. As for the location of poles in the complex energy sheets, we refer the readers to Ref. [7] where they are nicely illustrated.

We discovered that poles also exist near the ΛN threshold. In Table II, the antibound-state poles below the ΛN threshold are shown for the ${}^1S_0$ and ${}^3S_1 - {}^3D_1$ waves. The ${}^1S_0$ poles are relatively close to the threshold, and as expected correlate to the scattering length. As mentioned earlier, the ΛN scattering lengths have yet to be determined because of scant cross section data. However, the analyses of the hypertriton [2,3,21] constrain the S-wave scattering lengths. The potentials NSC97f and NSC89 which reproduce both the hypertriton binding energy and the ΛN cross section data have a ${}^1S_0$ scattering length within -2.6 to -2.4 fm, and a ${}^3S_1$ scattering length within -1.7 to -1.3 fm. The corresponding position of the ${}^1S_0$ pole is at about $-0.27i$ fm^{-1} in the $q_1(\Lambda - N$ relative momentum) complex plane.

Finally, we would like to point out that the analyses of the kaon photoproduction processes, $d(\gamma, K^+)YN$ or ${}^3\mathrm{He}(\gamma, K^+)YNN$ offer a very promising way to clarify the effects caused by the YN final-state interaction around the ΛN and ΣN thresholds. These processes are experimentally feasible at TJLAB and SPring-8. Further, the interactions of the photon and K^+ meson with the baryons are comparatively weak, which enables one to formulate and calculate these reactions rather well. All the techniques and insights gained in this article are immediately applicable to those reactions and we plan to perform such calculations in the near future.

ACKNOWLEDGMENTS

We would like to thank W. Glöckle for discussions, and critical and helpful comments. We are also grateful to L. Anthony for proofreading the final manuscript.

REFERENCES

[1] K. Miyagawa and W. Glöckle, Phys. Rev. **C48**, 2576 (1993).
[2] K. Miyagawa, H. Kamada, W. Glöckle, and V. Stoks, Phys. Rev. **C51**, 2905 (1995).
[3] W. Glöckle, K. Miyagawa, H. Kamada, J. Golak and H. Witała, Nucl. Phys. **A639**, 297c (1998).
[4] E. Hiyama, M. Kamimura, T. Motoba, T. Yamada and Y. Yamamoto, Nucl. Phys. **A639**, 169c (1998).
[5] P.M.M. Maessen, Th.A. Riken, and J.J. de Swart, Phys. Rev. **C40**, 2226 (1989).
[6] A. Reuber, K. Holinde, and J. Speth, Czech. J. Phys. **42**, 1115 (1992); Nucl. Phys. **A570**, 543 (1994).
[7] A.M. Badalyan, L.P.KoK, M.I.Polikarpov, and Yu.A. Simonov, Phys. Rep. **82**, 31 (1982).
[8] T. Nagae, *Proceedings of the 25th INS International Symposium on Nuclear and Particle Physics with High-Intensity Proton Accelerators*, edited by T.K. Komatsubara, T. Shibata and T. Nomura (World Scientific, Singapore, 1997), p.265.
[9] T. Harada, S. Shinmura, Y. Akaishi, and H. Tanaka, Nucl. Phys. **A507**, 715 (1990); T. Harada, Nucl. Phys. **A547**, 165c (1992).
[10] I.R. Afnan and B.F. Gibson Phys. Rev. **C47**, 1000 (1993).
[11] J. Reinhold *et al.* Nucl. Phys. **A639**, 197c (1998).
[12] M.M. Nagels, T.A. Rijken, and J.J. de Swart, Phys. Rev. **D15**, 2547 (1977).
[13] M.M. Nagels, T.A. Rijken, and J.J. de Swart, Phys. Rev. **D20**, 1633 (1979).
[14] B.C. Pearce and B.F. Gibson Phys. Rev. **C40**, 902 (1989).
[15] Th.A. Riken, V.G.J. Stoks, and Y. Yamamoto, Phys. Rev. **C59**, 21 (1999).

[16] R.G. Newton, *Scattering Theory of Waves and Particles* (McGraw-Hill, New York, 1966)
[17] W. Glöckle, *The Quantum Mechanical Few-Body Problem* (Springer-Verlag, Berlin, 1983).
[18] M.L. Goldberger and K.M. Watson, *Collision Theory* (Wiley, New York, 1964)
[19] T. Takemiya, Prog.Theor. Phys, **48**, 1547 (1972); **49**, 1602 (1973).
[20] Ch. Elster, J.H. Thomas, and W. Glöckle, Few-Body Systems **24**, 55 (1998).
[21] K. Miyagawa (unpublished).
[22] R.H. Dalitz and A. Deloff, Czech. J. Phys. **B32**, 1021 (1982) and references therein.

TABLES

TABLE I. Poles near the ΣN threshold for the component ${}^3S_1 - {}^3D_1$ of the various force models. The positions of the poles are shown on the complex planes of the relative momenta in the ΛN and ΣN channels, q_1 and q_2, respectively. The corresponding center-of-mass energies are indicated by E.

model	$q_1\,(\mathrm{fm}^{-1})$	$q_2\,(\mathrm{fm}^{-1})$	E (MeV)
NSC97f	$(1.46, -0.04)$	$(-0.35, 0.15)$	$(2135.6, -3.89)$
NSC89	$(1.37, 0.01)$	$(-0.04, -0.39)$	$(2126.3, 1.07)$
ND	$(1.43, 0.01)$	$(-0.18, -0.08)$	$(2132.8, 1.07)$
NF	$(1.44, -0.02)$	$(-0.28, 0.12)$	$(2134.2, -2.49)$

TABLE II. Poles below the ΛN threshold. The scattering lengths indicated by a are also shown. See the caption to Table I for other details.

model	partial wave	$q_1\,(\mathrm{fm}^{-1})$	$q_2\,(\mathrm{fm}^{-1})$	E (MeV)	a (fm)
NSC97f	${}^1S_0$	$(0, -0.27)$	$(0, 1.47)$	$(2051.8, 0)$	-2.59
	${}^3S_1 - {}^3D_1$	$(0, -0.37)$	$(0, 1.49)$	$(2049.3, 0)$	-1.70
NSC89	${}^1S_0$	$(0, -0.28)$	$(0, 1.47)$	$(2051.5, 0)$	-2.48
	${}^3S_1 - {}^3D_1$	$(0, -0.45)$	$(0, 1.51)$	$(2046.8, 0)$	-1.32
ND	${}^1S_0$	$(0, -0.35)$	$(0, 1.49)$	$(2050.0, 0)$	-1.83
	${}^3S_1 - {}^3D_1$	$(0, -0.35)$	$(0, 1.49)$	$(2050.0, 0)$	-1.89
NF	${}^1S_0$	$(0, -0.31)$	$(0, 1.48)$	$(2050.8, 0)$	-2.19
	${}^3S_1 - {}^3D_1$	$(0, -0.36)$	$(0, 1.49)$	$(2049.7, 0)$	-1.83

FIGURES

FIG. 1. Complex ω plane into which the energy Riemann surface is mapped. The two numbers inside the square brackets indicate the quadrants to which q_1 and q_2 belong, respectively. (The relation between the energy E and the momenta q_1 and q_2 is given by Eq. (4.1).) The parentheses show whether q_1 and q_2 are positive, negative, positive imaginary, or negative imaginary, respectively. The bold line expresses the region where bound or scattering states exist if present.

FIG. 2. Shape of the ΛN elastic total cross section σ around the ΣN threshold in the case a nearby t-matrix pole is located in the region [4,2]. (The pole resides in the 2nd quadrant of q_2.) The cross sections σ given by Eq. (4.11) are plotted, (a) as a function of $|q_2|$ below the threshold, (b) as a function of q_2 above the threshold, and (c) as a function of E.

FIG. 3. Same as Fig. 2 but for the case a t-matrix pole is located in the region [1,3]. (The pole resides in the 3rd quadrant of q_2.)

FIG. 4. Same as Fig. 2 but for the case a t-matrix pole is located in the region [2,4]. (The pole resides in the 4th quadrant of q_2.)

FIG. 5. ΛN elastic total cross sections around the ΣN threshold as a function of Λ lab momentum. Predictions by the force models of the Nijmegen group NSC97f, NSC89, ND and NF are shown.

FIG. 6. Positions of the poles for the force models NSC97f, NSC89, ND and NF in the complex q_2 plane.

FIG. 7. Trajectory of the pole for the potential ND in the complex q_2 plane with the multiplied overall strength parameter λ.

Fig. 1

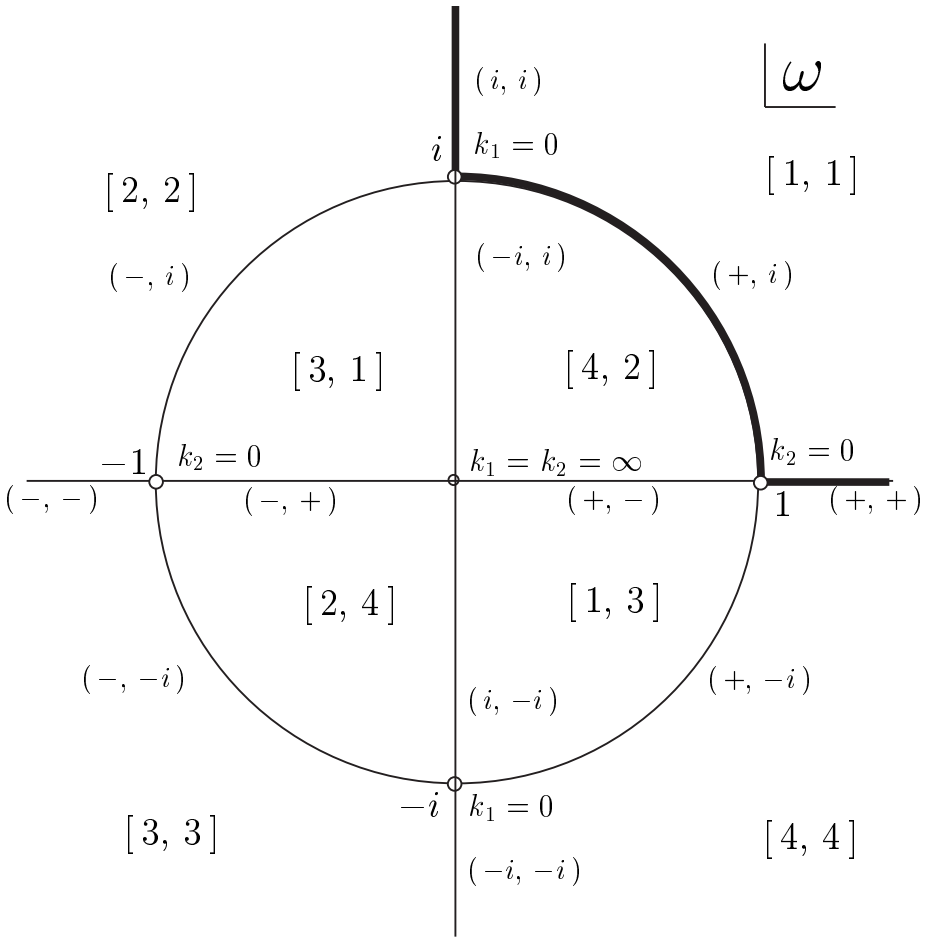
ω
$(i,\, i)$
i
$k_1 = 0$
$[\,1,\, 1\,]$
$[\,2,\, 2\,]$
$(-,\, i)$
$(-i,\, i)$
$(+,\, i)$
$[\,3,\, 1\,]$
$[\,4,\, 2\,]$
-1
$k_2 = 0$
$k_1 = k_2 = \infty$
$k_2 = 0$
$(-,\, -)$
$(-,\, +)$
$(+,\, -)$
1
$(+,\, +)$
$[\,2,\, 4\,]$
$[\,1,\, 3\,]$
$(-,\, -i)$
$(i,\, -i)$
$(+,\, -i)$
$-i$
$k_1 = 0$
$[\,3,\, 3\,]$
$[\,4,\, 4\,]$
$(-i,\, -i)$

Fig. 2

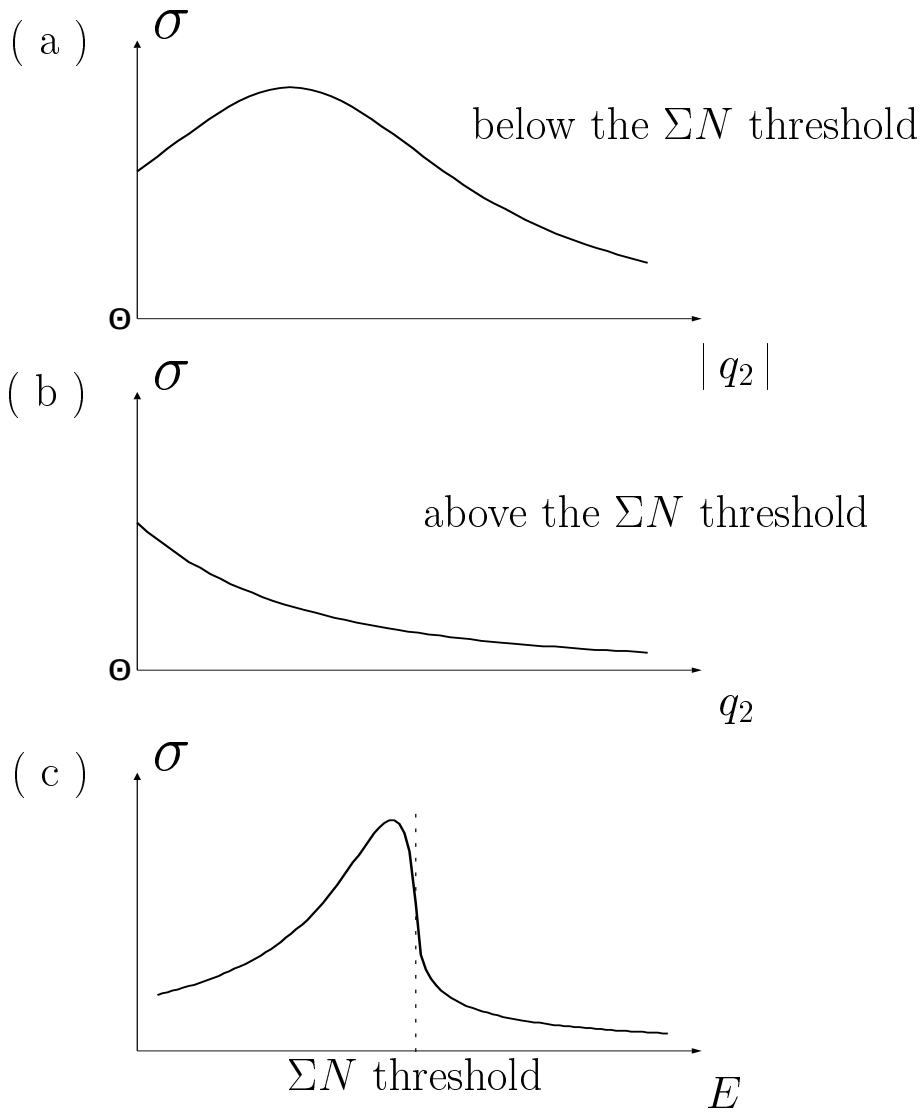
(a)
σ
below the ΣN threshold
0
$|\,q_2\,|$
(b)
σ
above the ΣN threshold
0
q_2
(c)
σ
ΣN threshold
E

Fig. 3

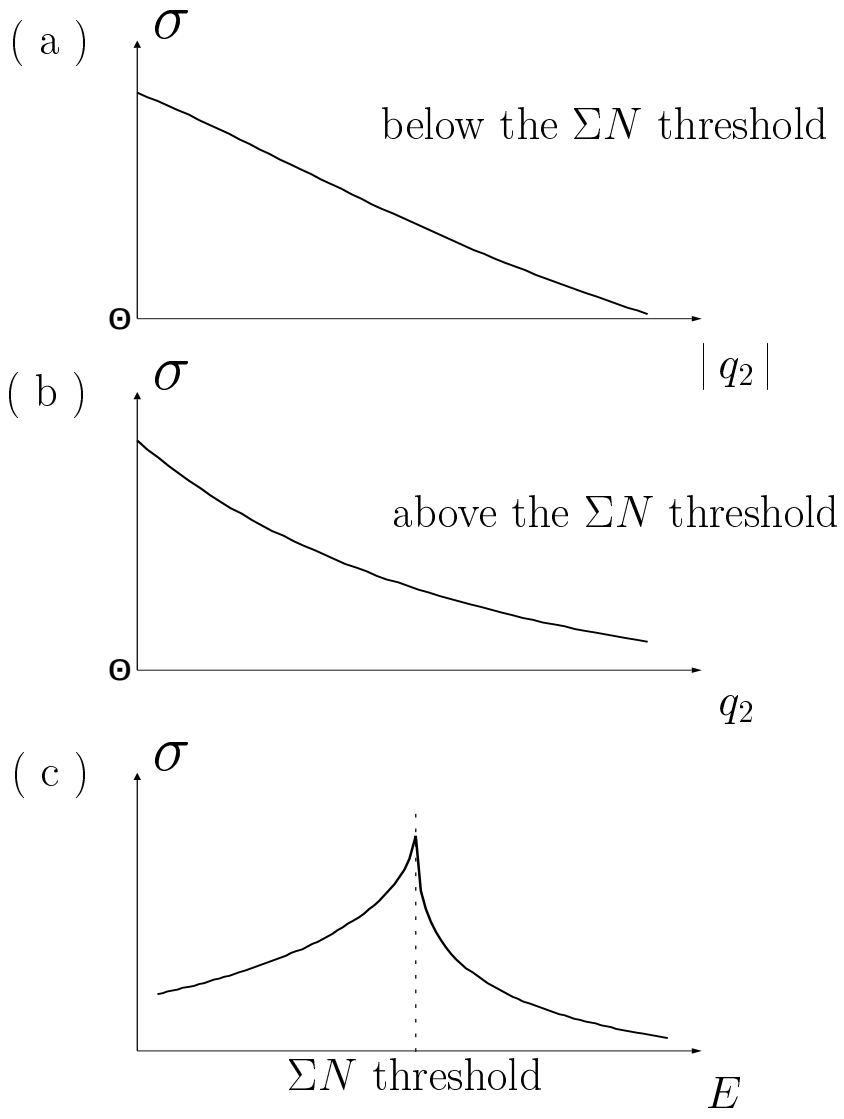
(a)
σ
below the ΣN threshold
0
| q2 |
(b)
σ
above the ΣN threshold
0
q2
(c)
σ
ΣN threshold
E

Fig. 4

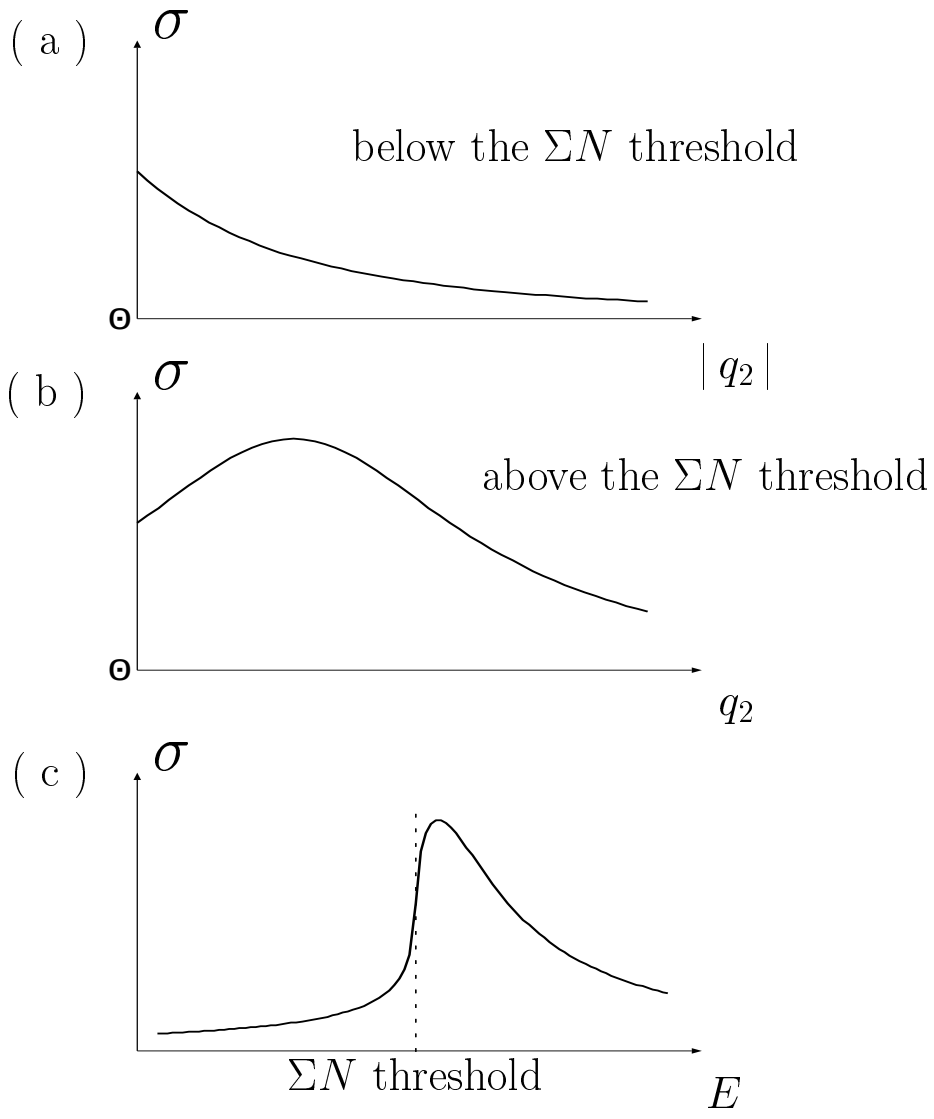
(a)
σ
below the ΣN threshold
0
| q2 |
(b)
σ
above the ΣN threshold
0
q2
(c)
σ
ΣN threshold
E

Fig. 5

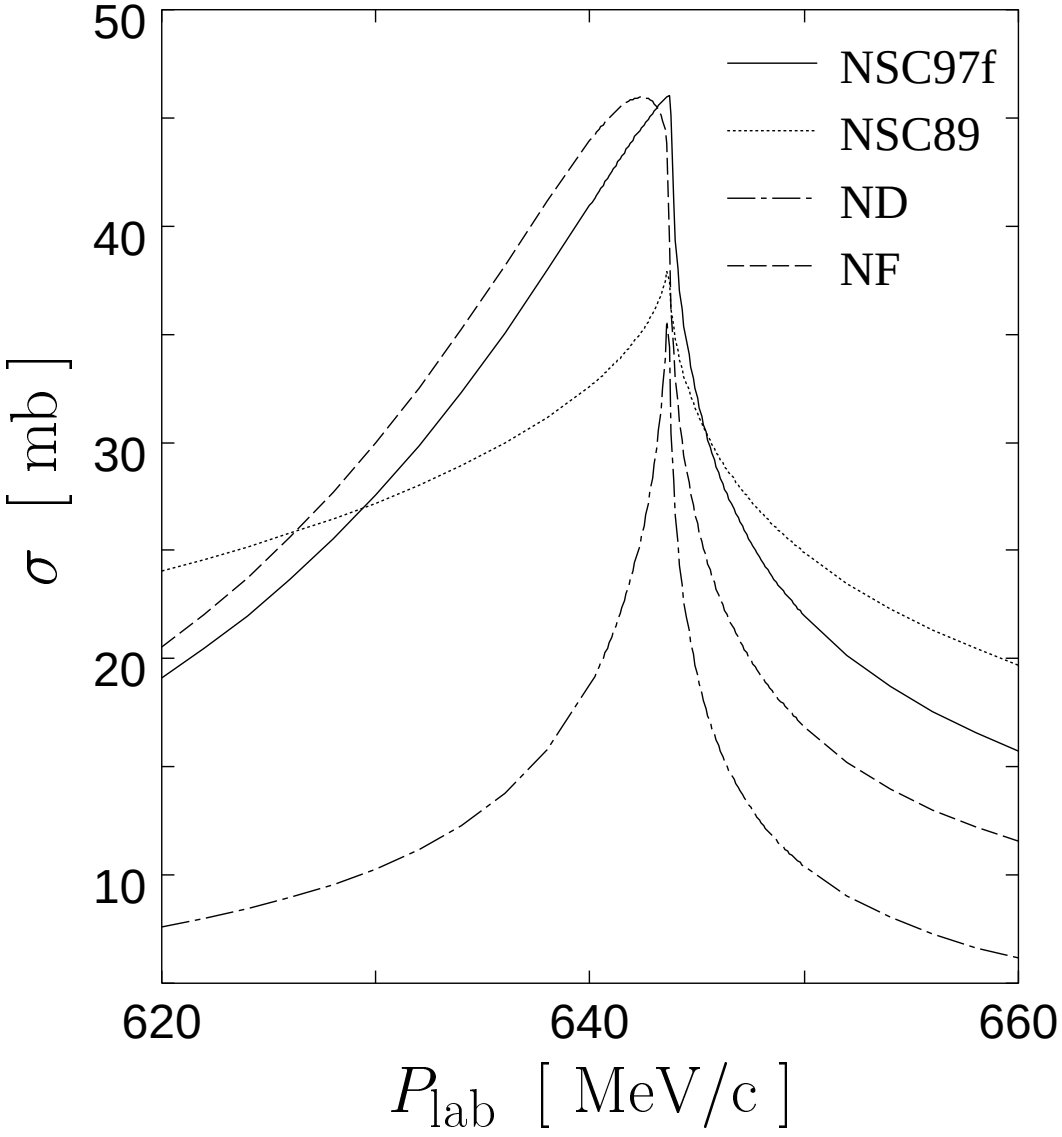
50
40
30
20
10
620
640
660
σ [mb]
$P_{\rm lab}$ [MeV/c]
NSC97f
NSC89
ND
NF

Fig. 6

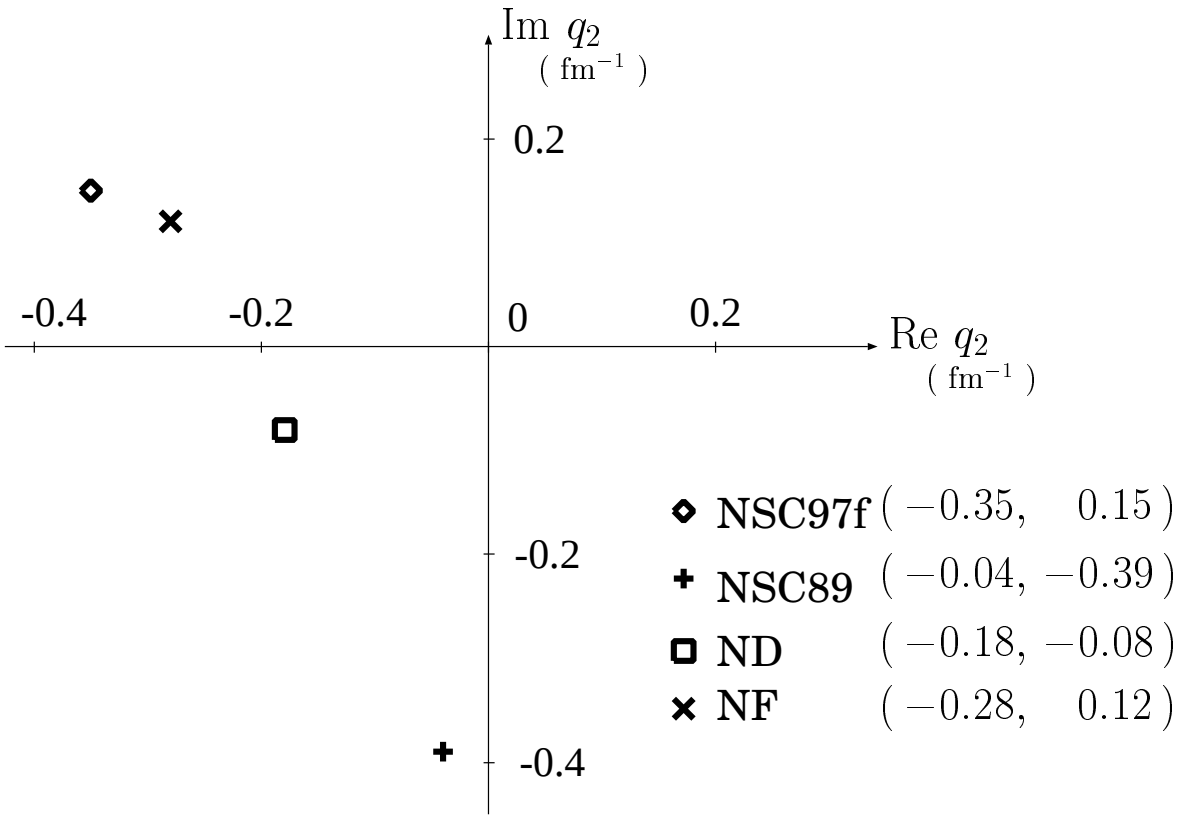
Im q_2
(fm^{-1})
0.2
-0.2
-0.4
0
0.2
Re q_2
(fm^{-1})
NSC97f (−0.35, 0.15)
NSC89 (−0.04, −0.39)
ND (−0.18, −0.08)
NF (−0.28, 0.12)

Fig. 7

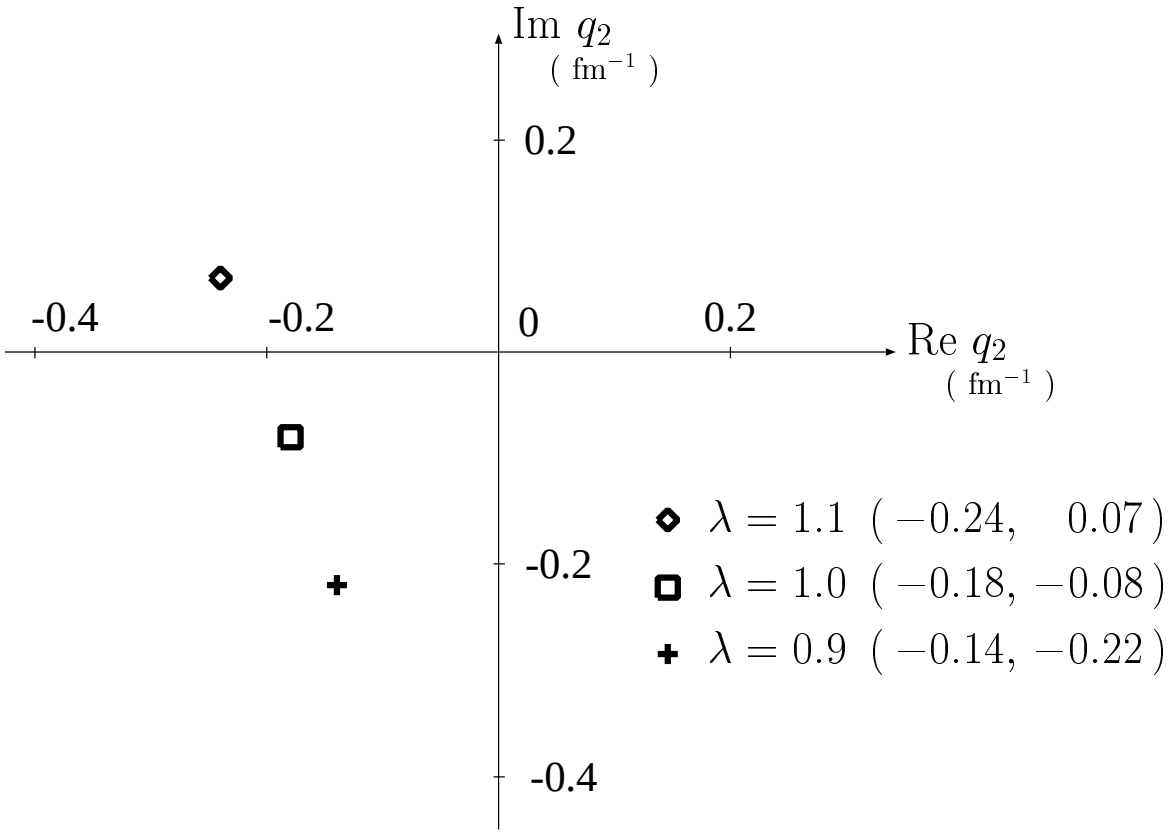
Im q_2
(fm^{-1})
0.2
-0.4
-0.2
0
0.2
Re q_2
(fm^{-1})
-0.2
-0.4
$\lambda = 1.1$ $(-0.24,\ \ 0.07)$
$\lambda = 1.0$ $(-0.18,\ -0.08)$
$\lambda = 0.9$ $(-0.14,\ -0.22)$